Theor. Comput. Fluid Dyn. (2014) 28:65–87
DOI 10.1007/s00162-013-0302-5

ORIGINAL ARTICLE

Mark Riherd · Subrata Roy · S. Balachandar

Local stability effects of plasma actuation on a zero pressure gradient boundary layer

Received: 10 October 2012 / Accepted: 29 March 2013 / Published online: 17 April 2013

Abstract The effects of plasma actuation in a flat plate boundary layer with zero pressure gradient have been simulated. Based on these simulations, non-dimensional parameters and a combined wall jet/boundary layer model of the velocity profile have been developed. A parametric study using local linear stability analysis has been performed to examine the hydrodynamic stability of the velocity profiles created through this model. Convective and absolute instability mechanisms are found to be important, some of which have not been previously documented. Neutral stability curves have been computed for the different instabilities, and when put in terms of the shape factor, they still compare favorably with reported canonical results, indicating that the critical Reynolds number is primarily a function of the shape factor. These results are also discussed in relation to existing experimental results as well as with respect to their implementation.

Keywords Hydrodynamic stability · Plasma actuators · Boundary layer control

1 Introduction

The process of a flow's transition to turbulence has long been a topic of study in fluid mechanics. Specifically, flows over flat plates with or without a pressure gradient are particularly important, as they share many characteristics with more complex flows. These flows can be described by the Falkner–Skan similarity solution, where the Blasius boundary layer is the special case of a zero pressure gradient (ZPG). Boundary layer flows such as these are prevalent on many types of air, ground, and marine vehicles, such as the flow over and around airfoils for fixed and rotating wing aircraft, the flat surfaces of automobiles and cargo trucks, and the sides and bottoms of ships. Reduction in the overall levels of drag on these different types of vehicles can lead to energy savings, allowing for more efficient and less costly operation, along with the associated benefits of reduced fuel consumption.

Stabilization or destabilization of a boundary layer flow can have a significant impact on the level of drag experienced by the body. Stabilizing the boundary layer decelerates the laminar to turbulent transition process. When attempting to reduce the level of friction drag experienced by a body, this is a beneficial course of action, as the drag associated with a laminar boundary layer is less than the drag associated with a turbulent boundary layer. However, when aiming to reduce the drag created by flow separation downstream, it is sometimes beneficial to accelerate the laminar to turbulent transition, as a turbulent boundary layer is more likely to remain attached than a laminar boundary layer. Additional flow control applications may exist with regard to heat transfer, chemical mixing, noise control, etc. where it may be prudent to stabilize or to destabilize the boundary layer, based on the problems specifications.

Communicated by O. Zikanov.

M. Riherd · S. Roy (✉) · S. Balachandar
Mechanical and Aerospace Engineering, University of Florida, Gainesville, FL 32611, USA
E-mail: roy@ufl.edu
Tel.: +352-392-9823

This study examines the effect of flow-wise (co-flow)- and flow-opposing (counter flow)-operated dielectric barrier discharge (DBD) actuators on the stability of the ZPG boundary layer flow. A DBD actuator consists of two electrodes asymmetrically separated from each other by a dielectric material. A high frequency ($\mathcal{O}$(kHz)), high potential ($\mathcal{O}(\mathrm{kV}_{pp})$) signal is applied to one electrode, while grounding the other. This potential difference generates a significant electric field and a weakly ionized plasma. Together, this electric field and the charged particles generate an electro-hydrodynamic body force, which can be used to add or remove momentum from the nearby fluid [1–3]. The addition (or subtraction) of momentum into (or from) the boundary layer suggests that DBD actuators operated in a continuous manner could be very useful for flow stabilization (or destabilization). Furthermore, these devices can be operated in a steady or duty-cycled manner, allowing them to be implemented as components of active and passive flow control systems. The primary restriction to the use of these actuator is their limited control authority. Under quiescent conditions, they are only able to generate wall jet flows up to 8–10 m/s.

There has been some previous work to use this type of actuator for boundary layer stabilization. Grundmann and Tropea [4–6] used these devices as a method of transition delay in an adverse pressure gradient boundary layer as part of a closed loop control system to cancel oncoming Tollmien–Schlichting (TS) waves. It was found that pulsed DBD actuators could be used to accurately inject momentum into the boundary layer, canceling the TS waves. Those researchers [5,6] also used the actuators in a flow-wise (co-flow) orientation with continuous actuation, constantly adding momentum into the boundary layer. Operating the actuators in this manner, they were able to delay the transition by 200 mm for a 10 m/s flow. Gibson et al. [7] used DBD devices in a steady manner in conjunction with boundary layer suction to reduce the displacement and momentum deficit boundary layer heights and stabilize the flow. Duchmann et al. [8] made PIV measurements of the TS wave in the region around the plasma actuator and showed a significant reduction in the wave amplitude and changes to the wave speed relative to the flow without plasma actuation.

Aside from experimentation, some theoretical work has also been performed describing how momentum addition, using electrical devices, modifies the boundary layer and its stability properties. Albrecht et al. [10] used LST and direct numerical simulation on a Lorentz force-induced actuation in a boundary layer flow, which showed that with a well-distributed body force mimicking wall suction, the transition can be significantly delayed. However, due to the more localized nature of the DBD actuator as compared to the Lorentz force actuator, the predicted global increase in stability may or may not be physically realizable. Limited spatial LST was performed and verified numerically and experimentally by Duchmann et al. [11] for a single condition where the flow-wise-oriented actuator was placed within the transitional Reynolds number regime, $Re_x \approx 270{,}000$ ($Re_{\delta^*} \approx 800$). While two operation modes for the plasma actuator were performed, an unsteady active wave canceling mode and a steady boundary layer modification mode, only the steady mode of operation was examined using LST in order to better explain the existing experimental results. That study also shows that there are distinct changes in the flow stability near the plasma device, but forgoes in-depth discussion of the effects. More complete stability analysis has recently been performed by Duchmann et al. [12] and Riherd and Roy [13]. Using local stability analysis and focusing on boundary layer profiles pulled from experiments [12] and CFD simulations [13], flow stabilization downstream of the plasma actuator is predicted to occur. Furthermore, though the assumptions required for a local stability analysis are ignored in the analysis, preliminary stability analysis suggests that multiple actuators grouped together as part of an array may be useful for much more significant delay of transition than single actuator [12].

With regard to specific applications beyond a flat plate, Séraudie et al. [14] have examined the effects of using DBD plasma actuators for the flow over an ONERA-D airfoil at an angle of attack (which generated an adverse pressure gradient over a majority of the chord). Their study employed low velocity wind tunnel testing and LST to predict the transition points of the flow, using a model similar to what has been developed in this study. Very recently, flight tests using continuous plasma actuation have been performed [9]. These flight tests demonstrated a transition delay of 3 % of the chord length for a small aircraft (a G109b motorized glider) for a high Reynolds number flow ($Re_x \approx 1.15 \times 10^6$).

The goal of this paper is to study how momentum injection and wall-jet-like effects stabilize or destabilize a boundary layer. While previous studies have considered the global effects of the plasma actuation, this study primarily aims to examine the local effects of momentum injection into the boundary layer over a wide range of parameters. This study also aims to frame the stability properties of the boundary layer in a manner based on the physical characteristics of the velocity profiles.

In Sect. 2, direct numerical simulations are performed of a laminar boundary layer with plasma actuation. A model of the baseline flow of a plasma-induced wall jet within a boundary layer is developed, based on the

results of these direct numerical simulations. The characteristics of the model are described, and the existence of instability modes in addition to the TS wave is hypothesized.

Boundary layer profiles generated by this model are then examined parametrically in Sect. 3 to determine how the local stability of the boundary layer is changed with the magnitude and orientation of plasma actuation. The necessary assumptions are quantified. Stability properties of boundary layer profiles from the simulations and the model are compared. Co-flow and counter flow actuations are both examined. The latter has not yet seen significant attention in terms of stability analysis in the existing literature. Evidence for the additional instability modes is found based on local stability analysis. Neutral stability curves are computed for all three types of instabilities with respect to the strength of the plasma actuation and the critical Reynolds number. Depending on how the effects of actuation are applied, the critical Reynolds number of the boundary layer is found to vary from an order of magnitude lower to an order of magnitude higher than that of the Blasius boundary layer. For a range of boundary layer profiles where the momentum addition or subtraction does not overpower the boundary layer profile, these results compare favorably with the universal correlation of Wazzan et al. [15].

In Sect. 4, the present results are discussed in relation to previous experimental results, as well as with regard to applications. Discrepancies between experiments and the stability analysis are discussed and reconciled. The effects of the unsteady body force with respect to flow stability is also discussed, predicting rough bounds on when the actuator may generate unstable perturbations in addition to modifying the flow stability properties of the boundary layer.

2 Development of a baseline flow model

All types of linear stability analysis require a base flow to examine. While specific flows can be very useful, especially when comparing numerical and experimental results, when attempting to examine flow physics over a wider parameter space, it is often useful to generate a simplified model of the flow, which does not have to be simulated or experimentally created every time a parameter is changed. Even so, simplified models must be based on realistic flows.

As a starting point to examine the effects of DBD actuation on a ZPG boundary layer, this flow is simulated numerically. This was done using a compressible Navier–Stokes solver, FDL3DI [16]. For the present simulations, the flow features are all fully resolved and the simulations can be considered a direct numerical simulation.

$$\frac{\partial \mathbf{Q}}{\partial t} + \frac{\partial}{\partial \xi}\left(\mathbf{F} - \frac{1}{Re}\mathbf{F}_v\right) + \frac{\partial}{\partial \eta}\left(\mathbf{G} - \frac{1}{Re}\mathbf{G}_v\right) = D_c\mathbf{S} \tag{1}$$

The dependent variables are defined as

$$\mathbf{Q} = \frac{1}{\mathscr{J}}\left[\rho,\ \rho u,\ \rho v,\ \rho E\right]^T \tag{2}$$

with the inviscid and viscid fluxes are defined using summation notation as

$$\mathbf{F} = \frac{1}{\mathscr{J}}\begin{bmatrix} \rho U \\ \rho u U + \xi_x p \\ \rho v U + \xi_y p \\ \rho E U + \xi_{x_i} u_i p \end{bmatrix},\ \mathbf{G} = \frac{1}{\mathscr{J}}\begin{bmatrix} \rho V \\ \rho u V + \eta_x p \\ \rho v V + \eta_y p \\ \rho E V + \eta_{x_i} u_i p \end{bmatrix} \tag{3a}$$

$$\mathbf{F_v} = \frac{1}{\mathscr{J}}\begin{bmatrix} 0 \\ \xi_{x_i}\tau_{i1} \\ \xi_{x_i}\tau_{i2} \\ \xi_{x_i}(u_j\tau_{ij} - Q_i) \end{bmatrix},\ \mathbf{G_v} = \frac{1}{\mathscr{J}}\begin{bmatrix} 0 \\ \eta_{x_i}\tau_{i1} \\ \eta_{x_i}\tau_{i2} \\ \eta_{x_i}(u_j\tau_{ij} - Q_i) \end{bmatrix} \tag{3b}$$

and the right-hand side source term is defined as

$$\mathbf{S} = \frac{1}{\mathscr{J}}\left[0,\ f_x,\ f_y,\ uf_x + vf_y\right]^T \tag{4}$$

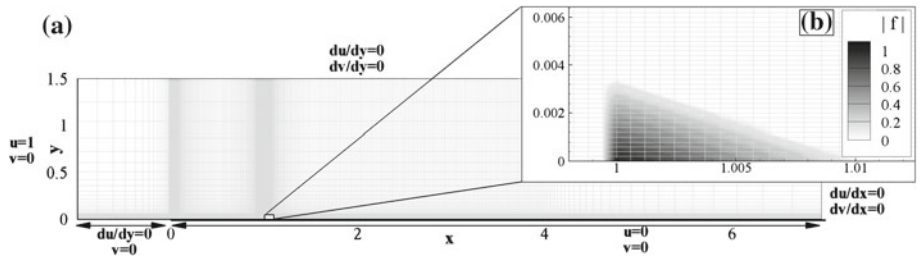

Fig. 1 **a** The two-dimensional domain and boundary conditions used for the *baseline* flow modifications, and **b** a close-up of the co-flow-oriented body force used within the boundary layer. Every other grid point is shown

where

$$E = \frac{T}{\gamma(\gamma-1)M_\infty^2} + \frac{1}{2}(u^2+v^2) \tag{5a}$$

$$Q_i = -\left(\frac{1}{(\gamma-1)M_\infty^2}\right)\left(\frac{\mu}{Pr}\right)\frac{\partial \xi_j}{\partial x_i}\frac{\partial T}{\partial x i_j} \tag{5b}$$

$$\tau_{ij} = \mu\left(\frac{\partial \xi_k}{\partial x_j}\frac{\partial u_i}{\partial x i_k} + \frac{\partial \xi_k}{\partial x_i}\frac{\partial u_i}{\partial x i_k} - \frac{2}{3}\delta_{ij}\frac{\partial \xi_l}{\partial x_k}\frac{\partial u_k}{\partial x i_l}\right) \tag{5c}$$

$$U = \frac{\partial \xi}{\partial x_i}u_i,\ V = \frac{\partial \eta}{\partial x_i}u_i \tag{5d}$$

In this system of equations, ρ represents the fluid density, u and v are the flow velocities, p is pressure, and E is the specific energy. All of these variables are non-dimensionalized by their reference values. Pressure is the exception to this, as it is non-dimensionalized by the dynamic head ($\rho_\infty u_\infty^2$). τ_{ij} represents the stress tensor and Q_i is the heat flux vector. f_x and f_y describe the normalized, spatially varying body force. The magnitude of this body force is modulated by the value of D_c.ξ and η represent the body-fitted coordinate system, $\mathscr{J}$ is the grid jacobian, U and V are the body-fitted velocities. The ideal gas law is also used in order to close the system of equations. While this is the compressible form of the Navier–Stokes equations, incompressible flow can be solved by setting the Mach number to an appropriately low value. It has been determined that a value of $M_\infty = 0.1$ provides a reasonable balance of incompressibility and numerical stability. At this Mach number, variations to the fluid density are less than 1 % throughout the domain. Temperature (and viscosity via Sutherland's law) variations are similarly small. As such, an incompressible approach to the flow stability should be sufficient.

The pressure and velocity variables that have no additional markings should be taken as instantaneous values. Those with an over bar, $(\bar{\cdot})$, should be understood to be steady values, and those with a tilde or prime marker, $(\tilde{\cdot})$ or $(\cdot')$, should be interpreted as referring to an eigenmode. Furthermore, while these numerical simulations of the flow performed using FDL3DI are instantaneous in nature, due to a lack of external perturbations, the flow fields generated do converge to a steady-state flow after running for a sufficient amount of time.

A fine, two-dimensional mesh (801 × 151) is used as a domain for the simulation. This domain is non-dimensionalized by the length from the leading edge of the plate to the actuator location. The domain extends upwind one unit of length from the leading edge of the plate and downwind 7 units of length. This mesh resolves the near-wall boundary layer, the effects near a sharp leading edge (but not the leading edge itself), and the steady addition of momentum through a body force term. Sufficiently far upstream of the leading edge, downstream of the actuator location, and as the mesh approaches the free stream, the mesh is coarsened in order to prevent unsteady effects from reflecting off of the boundary conditions. At the location of the plasma actuator ($x = 1$, $Re_x = 100{,}000$), 62 points are used to resolve the boundary layer height ($\delta_{99\,\%}$). This mesh is quite adequate for resolving the flow details near regions of high gradients, particularly for the thin boundary layer near the plate leading edge. A schematic of the domain is shown in Fig. 1. Parameters of the simulations are given in Table 1.

Presently, the effects of plasma actuation are modeled using a phenomenological model of the plasma body force [17] (Fig. 1b). Though improved body force models exist, based on first principles [18,19], experimental results [20,21] or reduced order models [22,23], the focus of this study is on the fluidic effects that the actuator

Table 1 Dimensional and non-dimensional values used to compute the base flow

Reference parameter	Value
Dimensional values	
u_∞	7.5 m/s
L	0.20 m
ρ_∞	1.20 kg/m^3
ν	1.5×10^{-5} m^2/s
Non-dimensional values	
Re	100,000
Pr	0.72
Ma	0.1
D_C	Varies, see Fig. 2a

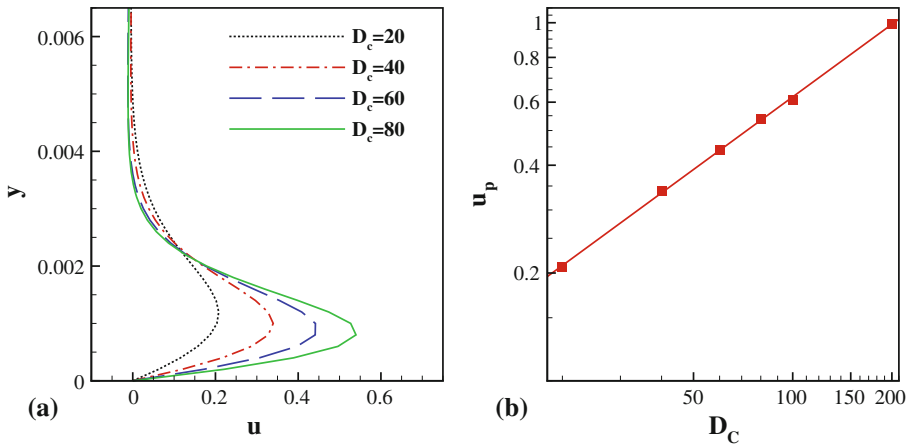

Fig. 2 **a** The velocity profile of the wall jet under quiescent conditions at $x = 1.01$ and **b** values of u_p generated by an actuator with a body force magnitude of D_C

creates, not plasma kinetics. As such, the primary purpose of the body force is to inject momentum into the flow over a specified area, which these different models do sufficiently well, though localized differences in the resulting velocities fields do exist. A comparison of several different models has been performed by Maden et al. [23], in which most of the models are found to generate a comparable wall jet profile at the end of the body force region (Fig. 5 in that paper). As the phenomenological model is the simplest of these to implement, it was selected for use in this study. However, to minimize against any errors due to the selection of this body force model, no data from inside of this region is used as part of any stability calculations.

The magnitude of the body force required to produce a wall jet under quiescent conditions of a specified velocity is determined a priori to the boundary layer simulations. The same code and mesh are used with no-slip conditions along the length of the lower and left side boundaries, and no-shear conditions over the other boundaries, leading to a quiescent condition over a majority of the domain, except for a wall jet in the vicinity of the plasma actuator (Fig. 2a).

The effect of the actuation on the flow is then characterized by the maximum velocity seen in the wall jet ($\bar{u}_p$) at the downstream edge of the body force ($x = 1.01$, shown in Fig. 2b). These simulations are then used to calibrate the value of D_c in Eq. 1 to use in the direct numerical simulations to generate a wall jet in the boundary layer of sufficient magnitude. The magnitude of the implemented force is characterized by the non-dimensional parameter

$$\gamma_0 = \frac{\bar{u}_p\big|_{x_0,\text{quiescent}}}{\bar{u}_\infty} \tag{6}$$

This parameter is selected in order to focus solely on the fluid dynamic effects of the plasma actuation and its influence on the flow stability, ignoring the electrical inputs such as voltage, frequency, and waveform into the device itself.

While these simulated flows allow for analysis under these specific flow scenarios, knowledge of the stability of a boundary layer modified by an arbitrary level of plasma actuation is also desirable. In order to

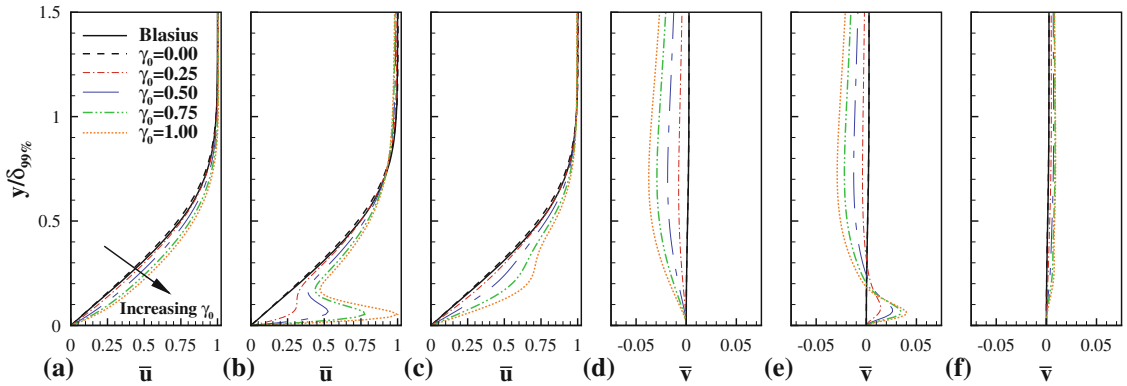

Fig. 3 Boundary layer velocity profiles as a function of γ at **a**, **d** locations upstream ($x = 0.99$), **b**, **e** directly downstream ($x = 1.01$) and **c**, **f** downstream ($x = 1.1$) of the actuator (located at $x = 1$). **a**–**c** show u and **d**–**f** show v. The rapid development of suction and wall jet effects and the gradual diffusion of momentum in the boundary layer can be seen to increase in magnitude as the value of γ is increased

examine the effects of a more general modified boundary layer, a reduced order model must be developed. It is known that under quiescent conditions, plasma actuation is able to create wall jets, which match the Glauert wall jet similarity solution sufficiently far downstream [24]. The current simulations (Fig. 3) as well as past results [2,3] suggest that the momentum addition into the boundary layer can form wall-jet-like effects if the levels of actuation are high enough. Even for lower levels of actuation, the momentum addition is still seen. This suggests that a superposition of a boundary layer and wall jet velocity profile should suffice to approximate the effects of plasma actuation on a ZPG boundary layer. That is,

$$\bar{u}_{\text{comb.}} = \bar{u}_{\text{BL}} + \bar{u}_{WJ} \tag{7}$$

In order to manipulate this model, base flow solutions for the boundary layer and wall jet profiles are necessary, as well as two non-dimensional parameters in order to scale the size and velocity magnitude of the momentum injection relative to the boundary layer. The Blasius boundary layer [25] and Glauert wall jet [26] similarity solutions are logical choices for the ZPG boundary layer, though there is no suggestion that the superposition of these solutions will result in an actual solution to the Navier–Stokes equations, only an approximation.

Concerning the non-dimensional parameters, while the global value of γ_0 can be used to characterize an entire two-dimensional flow field, but when examining individual boundary layer profiles it is more useful to define a localized velocity ratio parameter,

$$\gamma = \frac{\bar{u}_p\,(x)}{\bar{u}_\infty}. \tag{8}$$

which is more closely tied to the momentum addition that exists in the boundary layer profile downstream of the plasma actuator. This locally varying value of γ is a function of the global magnitude of the momentum injection (as characterized through γ_0) as well as the convective and diffusive transport of the momentum in the boundary layer, which will vary as one moves away from the actuator location. The momentum injected by the wall jet

$$\delta_p^* = \int_0^\infty \frac{\bar{u}_{WJ}\,(y)}{\bar{u}_p}\mathrm{d}y \tag{9}$$

and momentum deficit of the boundary layer (i.e., the displacement boundary layer height) can be formulated as length scales

$$\delta_{\text{BL}}^* = \int_0^\infty 1 - \frac{\bar{u}_{\text{BL}}\,(y)}{\bar{u}_\infty}\mathrm{d}y \tag{10}$$

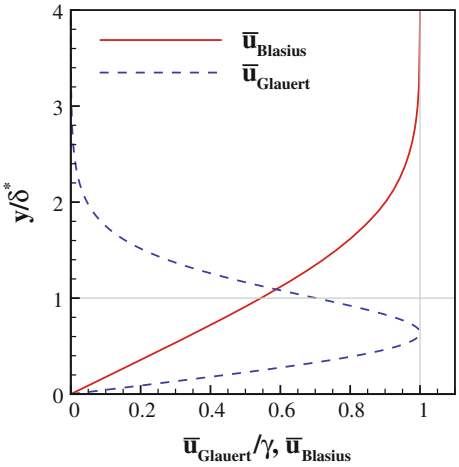

Fig. 4 Components of the flow model

to form a relative length scale such that

$$\eta = \frac{\delta_p^*}{\delta_{\mathrm{BL}}^*} \tag{11}$$

which is a local parameter, due to the development of the boundary layer and wall jet components in the flow. These non-dimensional parameters can then be applied to the initial model from Eq. 7 such that

$$\bar{u}\,(y) = \bar{u}_{\mathrm{Blasius}}\,(y) + \gamma \bar{u}_{\mathrm{Glauert}} \left(\frac{y}{\eta}\right) \tag{12}$$

The product of the two non-dimensional parameters developed here can be used to generate a third physically important parameter, μ, where

$$\mu = \eta\gamma \tag{13}$$

this parameter is the ratio of the momentum injected into the boundary layer by the plasma body force as compared to the momentum deficit in the boundary layer. While the total amount of momentum replaced is definitely important, it also matter exactly how this momentum is added into the boundary layer. Momentum addition outside of the boundary layer will not likely be helpful, nor will momentum addition that occurs at too localized of a location near the surface. Therefore, it is not only the velocity ratio or total momentum addition that will affect the boundary layer stability, but both of these parameters, improper application of which could be counter productive (Fig. 4).

Applying this model, a wide range of potential boundary layer profiles can be created. These boundary layer profiles are approximately matched to specific parameters from the simulations performed. The results of this show that there is a reasonably good agreement between the velocity profiles created by the model and those from the CFD simulations (Fig. 5a, b). Agreement is best near the wall, near the region of maximum velocity, and into the far field. However in the intermediate region where the wall jet dissipates momentum into the boundary layer, there is a noticeable discrepancy. As this discrepancy appears to be diffusive in nature, it is likely to vary depending on the local Reynolds number of the boundary layer velocity profile, which is not something that the current model takes into effect. There also appears to be a discrepancy in the inflection points between the model and the extracted boundary layer profiles, as shown using the second derivative of the velocity profile in Fig. 5c. The inflection points in the model velocity profiles do not occur in the same location in the boundary layer as those in the simulated velocity profiles, though they are still within $0.25\delta_{\mathrm{BL}}^*$. This discrepancy in the location of boundary layer inflection points has implications with respect to the existence and importance of inviscid instabilities to the boundary layer. This discrepancy seems to be smaller farther downstream of the actuator location, as the local value of the boundary layer ratio, η, has increased and the velocity ratio, γ, has decreased. As one moves farther and farther downstream of the actuator, the trends of η increasing and γ decreasing continue, due to the dissipation of momentum away from the wall.

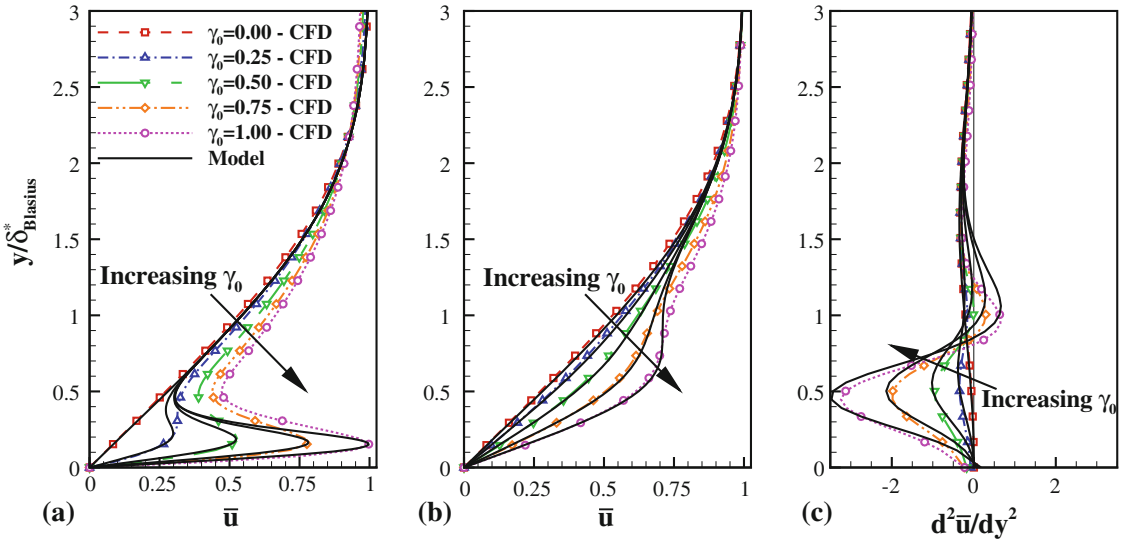

Fig. 5 Comparisons between the simulated and combined wall jet/boundary layer model of the velocity profiles are shown for the downstream profiles at **a** $x = 0.01$ and **b** $x = 1.1$ presented in Fig. 3. The values of γ_0 listed indicate which CFD simulation the velocities fields are being extracted from and matched to. The values of γ and η vary in order to fit to the model. **c** A comparison of the second derivative of $\bar{u}$ at $x = 1.1$ for the boundary layer profiles extracted from the CFD and generated by the model

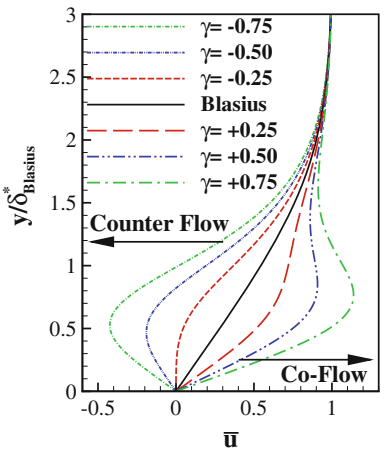

Fig. 6 Some of the boundary layer profiles used in the calculations $\eta = 1.0$ and varying values of γ

Agreement between the boundary layer profiles is better farther downstream of the actuators (at $x = 1.1$, as compared to $x = 1.01$, Fig. 5a, b), where the boundary layer profiles do not exhibit a large overshoot due to momentum addition. The local parameters for the model are $\gamma < 0.91$ and $0.28 < \eta < 0.35$ at $x = 1.01$ (Fig. 5a) and $\gamma < 0.35$ and $0.9 < \eta < 1.1$ at $x = 1.1$ (Fig. 5b). The co-flow boundary layer profiles seen farther downstream of the plasma actuator are much more similar to those in the common literature than those seen very close to the plasma actuator, as such, calculations using the low-order model of the boundary layer profile will use comparable values of γ and η.

It should be noted that there are now two displacement boundary layer heights relevant to the boundary layer stability, both of which are important for different reasons. From a flow control perspective, the scaling based on the boundary layer component (δ^*_{BL}, i.e., the Blasius boundary layer) of the combined velocity profile is most relevant. Holding this boundary layer height constant, momentum can be added or subtracted from the flow and the changes in the boundary layer's stability properties can be examined. When it comes to understanding the relevant physics, the displacement boundary layer height based on the combined boundary layer velocity profile (δ^*) is more relevant, as it is this boundary layer height defined by the velocity profile (Fig. 6).

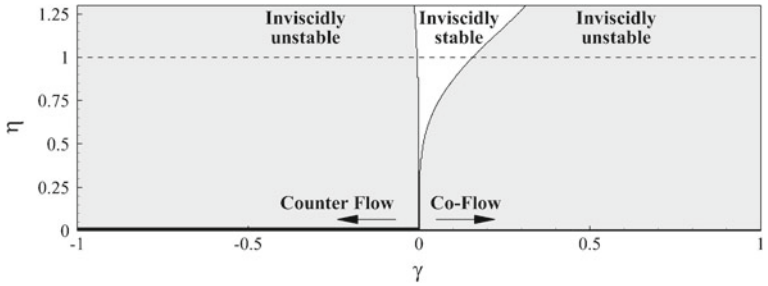

Fig. 7 Region where flow reversal occurs in the boundary layer profile

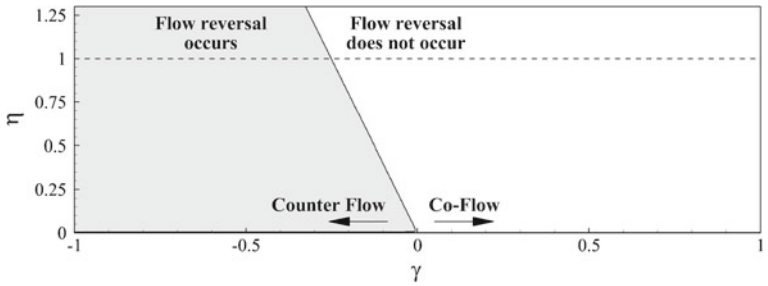

Fig. 8 Region where Fjørtoft's criterion is met

2.1 Additional instability modes

In addition to the viscid, convective instability associated with boundary layers (the TS mode), additional instabilities may also be present.

Previous studies of the effect of DBD actuation on boundary layer stability have focused on the co-flow orientation of the plasma actuation for flow stabilization. However, there do exist instances where flow destabilization is a preferable goal of flow control. In these instances, operating the plasma actuator in a counter flow manner may be of use. Just as co-flow actuation injects momentum into the boundary layer and stabilizes it, counter flow actuation removes momentum from the boundary layer and should destabilize the boundary layer. In addition to removing momentum, for high enough levels of counter flow actuation (that is large, negative values of γ), flow separation and reversal may occur. This flow reversal, while not a requirement of an absolute instability, suggests that one may be present, adding another instability mode to the existing convective instability associated with ZPG boundary layers. Flow regimes (w.r.t. γ and η) at which flow reversal may occur are shown in Fig. 7, which are evaluated using the present model of the plasma modified boundary layer profile.

Examining the different boundary layer velocity profiles generated by the simulation and the model, it can be seen that inflection points may occur in the velocity profile (Fig. 5c). While an inflection point does not necessarily indicate that an inviscid instability is present, it raises suspicions that one may exist. Fjørtoft's criterion is a stricter condition for the presence of an inviscid instability and is defined as

$$\frac{\partial^2 \bar{u}}{\partial y^2}\,(\bar{u}_S - \bar{u}) < 0 \tag{14}$$

where $\bar{u}$ is the steady-state wall tangential velocity, and $\bar{u}_S$ is the velocity at whatever inflection points may exist. Applying this criterion to the many boundary layer profiles computed for determining whether flow reversal had occurred, it can be seen that there is only a small region in the (γ, η) plane where Fjørtoft's criterion is not met (Fig. 8). This result suggests that the region for stabilizing flow control is limited and that only slight levels of co-flow actuation can be used for this purpose. If too large of a co-flow actuation is applied, then inviscid instabilities will become a significant problem.

3 Flow stability

The present analysis employs a local stability method, which requires the assumptions of a slowly developing, parallel flow. In order to quantify how appropriate these assumptions are, three parameters have been developed, $E_\parallel$, E_d, and E_κ. Using the already non-dimensionalized velocities and length scale (in this case, the displacement boundary layer height), the validity of the parallel flow assumption can be

$$E_\parallel = \max_{y\in(0,\infty)} \left(\tan^{-1} \left| \frac{\bar{v}}{\bar{u}} \right| \right) \tag{15}$$

which is the maximum angle of the flow a given point along the length of the boundary layer. The validity of the slowly developing flow assumption can be quantified using

$$E_d = \max_{y\in(0,\infty)} \left| \frac{\partial \bar{u}}{\partial x} \right| \tag{16}$$

which measures how rapidly the flow is developing. Another source of error, which does not see significant exposure when considering flat plate boundary layers, is that of the streamline curvature. This assumption can be quantified using derivative in the flow angle

$$E_\kappa = \max_{y\in(0,\infty)} \left| \frac{\partial \tan^{-1}\left(\frac{\bar{u}}{\bar{v}}\right)}{\partial x} \right| \tag{17}$$

All of these metrics are local parameters and can be applied at specific points along the length of the boundary layer (here indicated by Re_x). Furthermore, these values have all been dimensionalized with respect to the boundary layer height, not distance between the leading edge and the actuator location. As such, this should provide a better representation of these values with respect to the boundary layer.

Computing these metrics, it can be seen that the approximations necessary for the one-dimensional eigenvalue method are only invalid within several boundary layer lengths upstream and downstream of the plasma actuation (Fig. 9). This is good news, as it allows for the stability analysis to be applied over a majority of the flow field. This quantification of the assumptions shows that in the region of momentum injection, where the largest values of γ are expected to be found, the present model of hydrodynamic stability is weakened. In order to perform analysis in this region immediately around the plasma actuator, more sophisticated stability tools would need to be employed.

For smaller values of γ, the results of this model are expected to be quantitatively accurate. For the larger values of γ examined, the results are to be interpreted with care. Though the assumptions for the model are weakened, the results produced by the model are sensible within the hypotheses presented in Sect. 2.

3.1 Numerical model of the eigenvalue method

Linear stability theory can be used to predict the existence and growth rates of instabilities that may manifest in the boundary layer. Temporal instabilities are examined here for the reasons of computational simplicity and so that simplified one-dimensional model of the plasma influenced boundary layer can be employed, though a spatial analysis would be equally valid for these one-dimensional velocity profiles. The simulations performed in Sect. 2 suggest that while it does exhibit some rapid spatial changes near the actuator, this flow can be considered a slowly developing, nearly parallel flow over the remainder of the domain. As such, one-dimensional linear stability theory can be applied. Starting with the linearized Navier–Stokes equations,

$$u_i = \bar{u}_i + \tilde{u}_i,\ p = \bar{p} + \tilde{p} \tag{18a}$$

$$\frac{\partial \tilde{u}_i}{\partial x_i} = 0 \tag{18b}$$

$$\frac{\partial \tilde{u}_i}{\partial t} + \bar{u}_j \frac{\tilde{u}_i}{\partial x_j} + \tilde{u}_j \frac{\bar{u}_i}{\partial x_j} + \frac{\partial \tilde{p}}{\partial x_i} - \frac{1}{Re_{\delta_0^*}} \frac{\partial^2 \tilde{u}_i}{\partial x_j^2} \approx 0 \tag{18c}$$

The non-dimensionalization here is based on the displacement boundary layer height of the non-actuated case (δ^*_{BL}) at a given location in x rather than location of the actuator as it was done in the previous section.

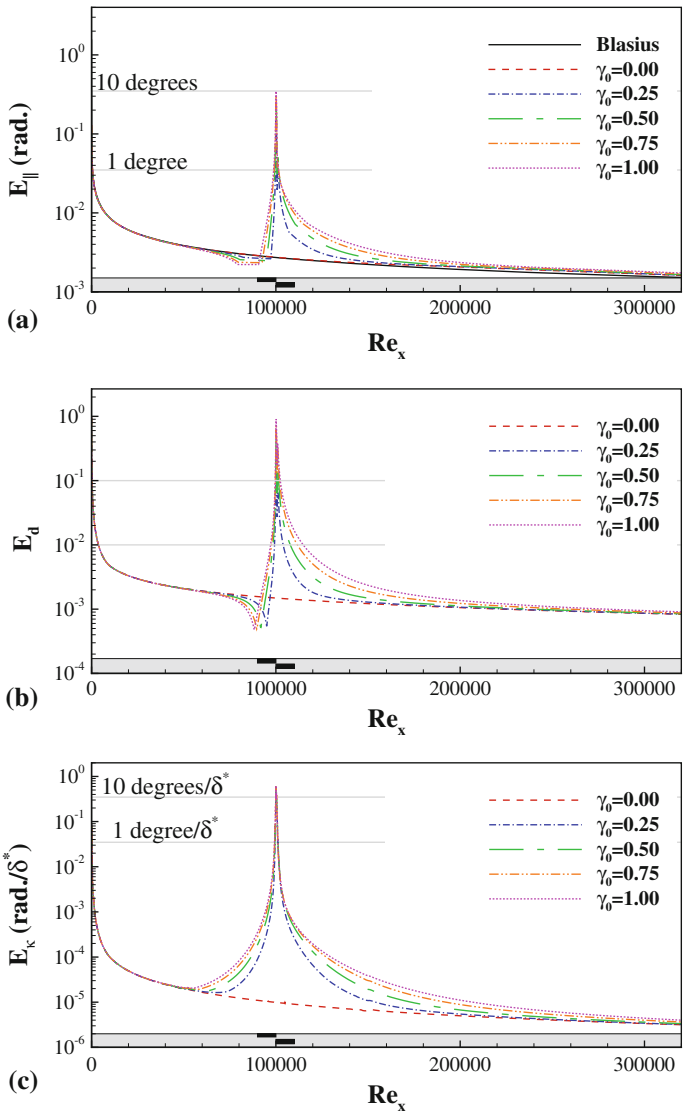

Fig. 9 Quantification of the **a** parallel, **b** slowly developing, **c** and streamline curvature assumptions for the computed flows with plasma actuation simulated at $Re_x = 100{,}000$. Actuator location is marked, though the size of the electrodes is exaggerated for clarity. The derivative terms are non-dimensionalized by the local displacement boundary layer height $\delta*_{\mathrm{BL}}$. Re_x should be interpreted as the location along the length of the boundary layer

The problem can be further simplified if several assumptions are made. Assume that all of the disturbance quantities are wavelike in nature and can be split into the product of a disturbance profile which varies in y and a traveling wave in x and z, such that

$$\tilde{\phi} = \phi'(y) \exp\left(i\left(\alpha x + \beta z - \omega t\right)\right) \tag{19}$$

where α, β, and ω are the angular wave numbers in x, z, and time, respectively, and that $i = \sqrt{-1}$. Also assume that a slowly developing flow can be approximated as a 1D mean flow ($v = w = \frac{\partial(\overline{\cdot})}{\partial x} = \frac{\partial(\overline{\cdot})}{\partial z} = 0$). Thus, the problem can be formulated as a generalized eigenvalue problem:

$$i\alpha u' + \frac{\partial v'}{\partial y} + i\beta w' = 0 \tag{20a}$$

$$i\alpha \bar{u} u' + v' \frac{\partial \bar{u}}{\partial y} + i\alpha p' - \frac{1}{Re}\left(-\alpha^2 u' + \frac{\partial^2 u'}{\partial y^2} - \beta^2 u'\right) = i\omega u' \tag{20b}$$

Table 2 Convergence of the critical eigenvalue for two sample cases. For both cases, $Re_{\delta^*,\text{Blasius}} = 1{,}000$, $\alpha = 0.3$

n_y	Blasius, ω_{TS}	Model ($\eta = 1$, $\gamma = 0.25$), ω_{Fast}
51	$0.11238325236 - 0.00090042619i$	$0.23306979831 + 0.00220664208i$
71	$0.11017358051 + 0.00059957882i$	$0.23281253531 + 0.00242939870i$
101	$0.10924347588 + 0.00163256137i$	$0.23273816623 + 0.00249039239i$
142	$0.10898287015 + 0.00213952218i$	$0.23272109814 + 0.00250492030i$
201	$0.10892701325 + 0.00235576622i$	$0.23271726363 + 0.00250853091i$
283	$0.10892058760 + 0.00243347102i$	$0.23271652043 + 0.00250929338i$
401	$0.10892145449 + 0.00246038133i$	$0.23271638394 + 0.00250945035i$
566	$0.10892233968 + 0.00246910010i$	$0.23271636662 + 0.00250947873i$
801	$0.10892273162 + 0.00247197532i$	$0.23271636809 + 0.00250948486i$

$$i\alpha\bar{u}v' + \frac{\partial p'}{\partial y} - \frac{1}{Re}\left(-\alpha^2 v' + \frac{\partial^2 v'}{\partial y^2} - \beta^2 v'\right) = i\omega v' \tag{20c}$$

$$i\alpha\bar{u}w' + i\beta p' - \frac{1}{Re}\left(-\alpha^2 w' + \frac{\partial^2 w'}{\partial y^2} - \beta^2 w'\right) = i\omega w' \tag{20d}$$

where ω are the eigenvalues and u', v', w', and p' are the eigenmodes of this system. All of these variables should be thought of as having complex values. The stability of this system and individual modes in the system are characterized by the imaginary part of ω, where $\omega = \omega_R + i\omega_I$. Should $\omega_I < 0$ for any particular eigenmode, then that mode is stable. Should $\omega_I > 0$ for any mode, then that mode and the entire eigensystem can be considered unstable.

This set of equations (Eqs. 20a–20d) is then discretized onto a uniform staggered mesh. A fourth-order accurate, centered finite difference stencil is used for the differencing over a majority of the domain. A second-order accurate, centered finite difference scheme is used at the boundaries. Boundary layer profiles from the model developed in Sect. 2 are interpolated onto the uniform mesh, which extends $4\delta_{99\,\%}$ ($\approx 11.6\delta^*_{\text{BL}}$) away from the wall.

3.1.1 Grid convergence

The appropriateness of the present local stability model is dependent on the satisfaction of the assumptions outlined in the previous section. When this model is appropriate, it must still be properly implemented. In order to check for the accuracy and convergence of the solution, a grid resolution study has been performed. Two separate cases, one examining the TS mode, the other examining a "fast" mode, which will be expanded upon in Sect. 3.3, have been examined. The convergence of the most unstable eigenvalue can be found in Table 2 and Fig. 10. The order of accuracy of the stencils employed for the calculations were second- and fourth-order accurate, respectively. The convergence of the unstable eigenmodes reflects this, as it converges at a rate between n_y^{-2} and n_y^{-4}.

Based on this convergence data, the grid resolution of $n_y = 201$, $\Delta y = 0.0581\delta^*_{\text{Blasius}}$ appears to be sufficient resolution for the present method.

3.1.2 Comparison between computed boundary layer profiles and the model

Before performing a large number of calculations, it would be beneficial to compare the stability properties of the computed boundary layer profiles with those generated by the model. This comparison would be beneficial in determining the validity of the present model for this type of calculation. For this calculation, the boundary layer profiles shown in Fig. 5b have been chosen for examination. At this point, $Re_x = 110{,}000$ and $Re_{\delta^*} = 556$. While these profiles may not be the most optimal due to their closeness to the plasma actuator, they exhibit enough variation in the boundary layer profile to determine whether or not the model and the computed boundary layer profiles predict similar behavior. The exact parameters used for the model are given in Table 3.

In comparing the result of the two models, it should be noted that both the eigenmodes and the eigenvalues should be considered, as they together predict the relevant physics. Comparing the eigenvalues (Fig. 11), it can be seen that the error of the real and imaginary components is less than 20 % of the magnitude of the critical eigenvalue, and for most of the comparison cases, it is less than 10 %, especially at higher wavenumbers.

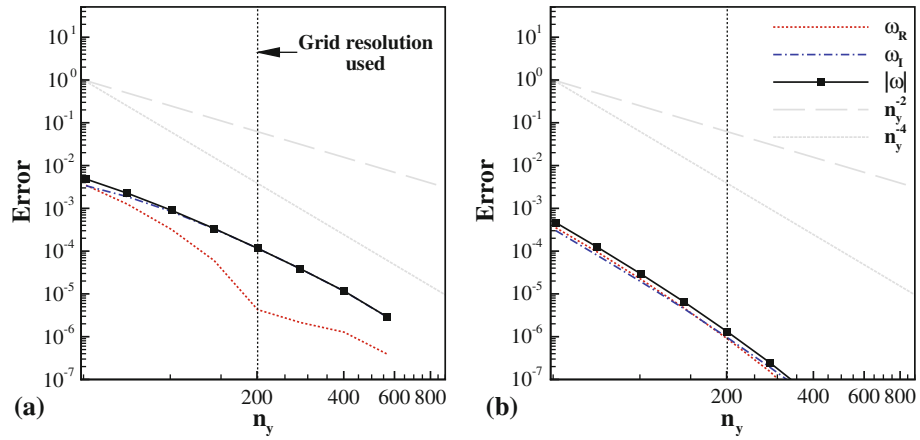

Fig. 10 Grid convergence for the cases of the **a** Blasius boundary layer profile and **b** a boundary layer profile generated by the model ($\eta = 1.0$, $\gamma = 0.25$). For both cases, $Re_{\delta^*,\text{Blasius}} = 1{,}000$, $\alpha = 0.3$

Table 3 Parameters of the model used to generate the approximated boundary layer profiles and to compare the stability properties of the computed and modeled boundary layer profiles

Case	γ	η
$\gamma_0 = 0.25$	0.0492	1.0502
$\gamma_0 = 0.50$	0.1264	0.9775
$\gamma_0 = 0.75$	0.2376	0.9045

Further comparing the results, it can be seen that the general trends of the frequency and growth rate with regard to the increase in the magnitude of the plasma actuation (increasing γ_0), as well as the streamwise wave number, are comparable for the boundary layer profiles extracted from the CFD simulations and for the model.

Examining the eigenmodes (Fig. 12), it can be seen that the general shape of the eigenmode is comparable for the boundary layer profiles extracted from the CFD simulations and those generated by the model. The trends of increased actuation are present, as the maximum value of $|u'|$ moves away from the wall and an indentation forms in the perturbation velocity profile near the wall for both sets of base flow velocity profiles. The model appears to amplify these trends more than the boundary layer profiles extracted from the CFD simulations, but the trend is present for both sets of velocity profiles.

3.2 Linear stability using the 1D flow model

In Sect. 2.1, it was suggested that a number of different effects could occur to the flow stability as a function of the local velocity ratio, γ. Different instabilities may occur, and significant changes to the nature of the instabilities may occur as the effect of the momentum injection is varied.

For these calculations, the model of the boundary layer flow developed in Sect. 2 is used (Eq. 7, some of the velocity profiles of which are shown in Fig. 6), as it affords more ease and flexibility in generating boundary layer profiles than a CFD based approach. Based on the quantification of the assumptions required for a local stability analysis based on Eqs. 15–17, this stability analysis should not examine any flows immediately around the plasma actuator, and should focus on regions farther away from the actuator.

In order to determine which instabilities may exist, a parametric study is presented in order to determine the effects of co-flow and counter flow actuation on the different eigenmodes of the boundary layer. The eigenvalues of the flow are computed for the case of $\eta = 1.0$ and $\alpha = 0.3$ for various Reynolds numbers and varying the level of actuation from $\gamma = -0.5$ to $\gamma = 0.5$ (Fig. 6). The value of γ for which the eigenvalues are computed has been varied slowly ($\Delta\gamma = 0.02$) in order to ensure that smooth behavior exists. The computed eigenvalues are shown in Fig. 13. It can be seen that at the lowest Reynolds number examined ($Re_{\delta^*} = 150$, Fig. 13a), that the most unstable mode for a given value of γ varies continuously as γ varies from -0.5 to 0.5. However, at a higher Reynolds number ($Re_{\delta^*} = 450$ and 600, Fig. 13c, d), the most unstable mode changes as the value of γ is increased from -0.5 to 0.5. At the higher Reynolds number, the TS mode becomes more

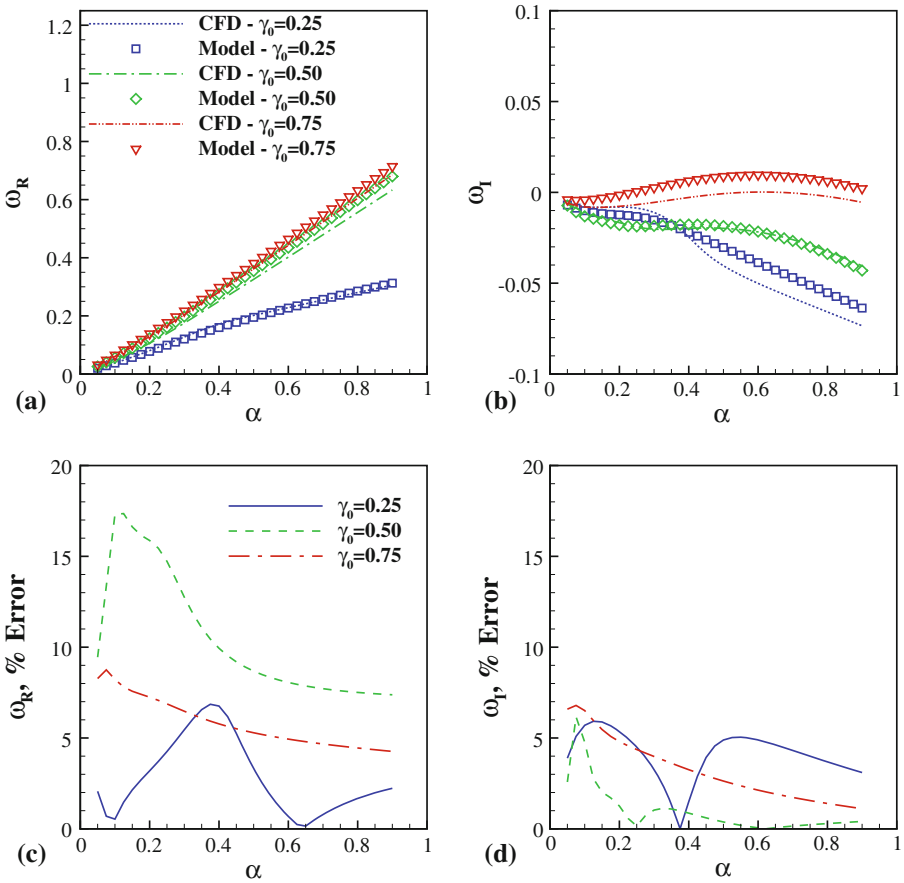

Fig. 11 Comparisons of the **a** real and **b** imaginary components of the critical eigenvalues and percentage error of the **c** real and **d** imaginary components of the eigenvalue for the boundary layer profiles extracted from the CFD simulations and the model of the boundary layer profile

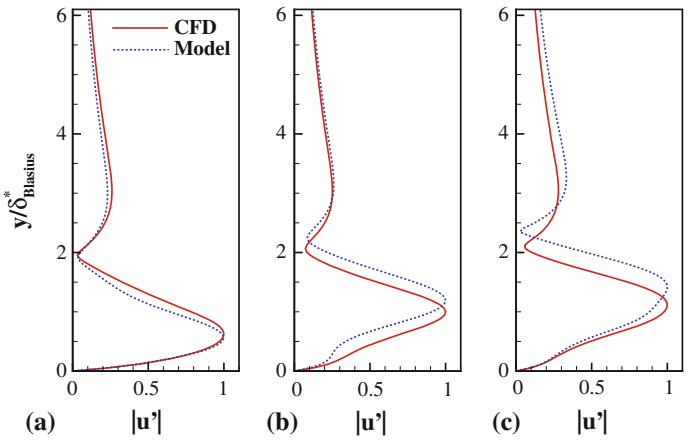

Fig. 12 Comparisons of the eigenmodes for **a** $\gamma_0 = 0.25$, **b** $\gamma_0 = 0.50$, and **c** $\gamma_0 = 0.75$ for $\alpha = 0.3$

stable as co-flow actuation is applied and is destabilized as counter flow actuation is applied. Even though the TS mode is stabilized as co-flow actuation is applied, a different mode, which had previously been very stable, becomes unstable as this type of flow control is utilized.

It could be assumed that these eigenmodes are moving in the complex plane as the dispersion relationship which controls them is varied with respect to the Reynolds number. However, it can be seen that these two

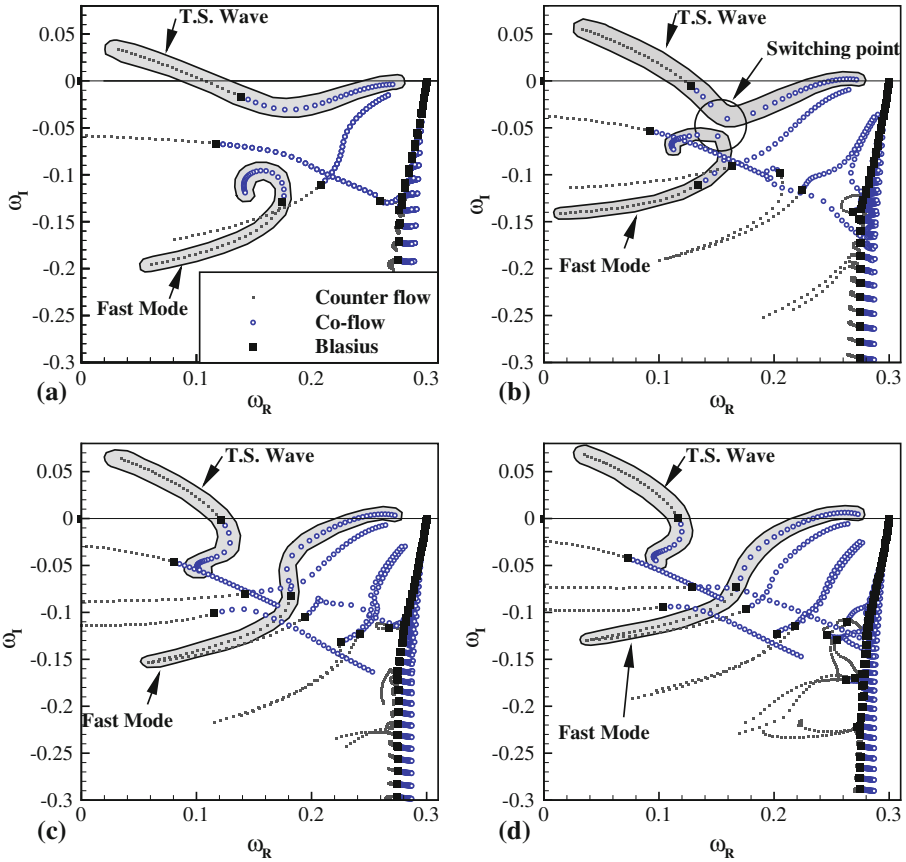

Fig. 13 Computed eigenvalues as a function of γ ($-0.5 < \gamma < 0.5$) at the wave number of $\alpha = 0.3$ and a boundary layer height ratio of $\eta = 1.0$ for **a** $Re_{\delta^*,\text{Blasius}} = 150$, **b** $Re_{\delta^*,\text{Blasius}} = 300$, **c** $Re_{\delta^*,\text{Blasius}} = 450$, and **d** $Re_{\delta^*,\text{Blasius}} = 600$. *Dots* indicate eigenvalues for a certain counterflow velocity profile. *Circles* indicate eigenvalues for a certain co-flow velocity profile

branches of the dispersion relationship intersect (Fig. 13b) and then trade portions of their branch to each other as the Reynolds number is changed. The critical point at which this occurs is $Re_{\delta^*,\text{Blasius}} = 315$ and $\gamma = 0.0675$ at the point $\omega = 0.155 - i0.495$ for the wavenumber $\alpha = 0.3$ (this value of α was not optimized to find the absolute lowest value of Re where this effect occurs). There may be a number of different implications with this branch switching. The implication most relevant to this study is that at very low Reynolds numbers, only a single eigenmode is relevant to the stability of these combined wall jet and boundary layer flows, but at moderate to high Reynolds numbers, two separate modes exist that are connected to each other.

3.3 Co-flow actuation

Examining the effects of co-flow actuation, it is expected that this manner of operation will stabilize the boundary layer up to a certain point, above which inviscid instabilities will become relevant and the flow will be destabilized. Neutral stability curves have been calculated for the cases of positive γ and are shown in Fig. 14. Two different scalings based on the displacement boundary layer height and the displacement height of Blasius component of the combined velocity profile are used. However, neither of these scalings provide a sufficient collapse of the data. These neutral stability curves confirm that there are two separate modes which can become unstable, with widely varying properties. For the case of co-flow actuation, these two modes can be separated as being a (slow) TS wave and a (fast) outer mode, based on the real phase speed ($c_R = \frac{\omega_R}{\alpha}$). Examining the velocity profiles of these waves (Fig. 15), it can be seen that the structure of the waves is different. The TS mode is not independent of the plasma actuation, but it does retain its basic shape as the magnitude of the wall jet is varied. The faster mode shows a stronger dependence on the plasma actuation. As

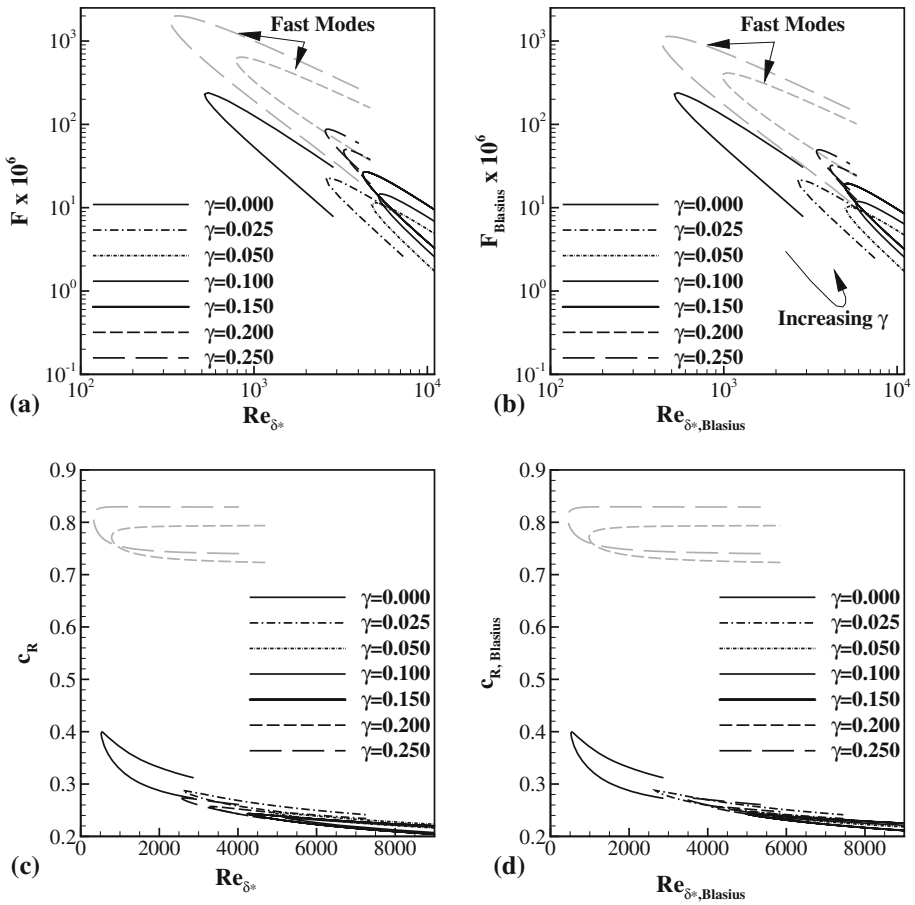

Fig. 14 Neutral stability *curves* in terms of the **a**, **b** reduced frequency, $F = \omega_R/Re$, and the **c**, **d** phase velocity, $c_R = \omega_R/\alpha$ scaled by the displacement boundary layer heights of the **a**, **c** combined velocity profile and the **b**, **d** Blasius component of the velocity component. The TS waves are indicated by the *solid lines*. The outer mode is indicated by the *gray lines*

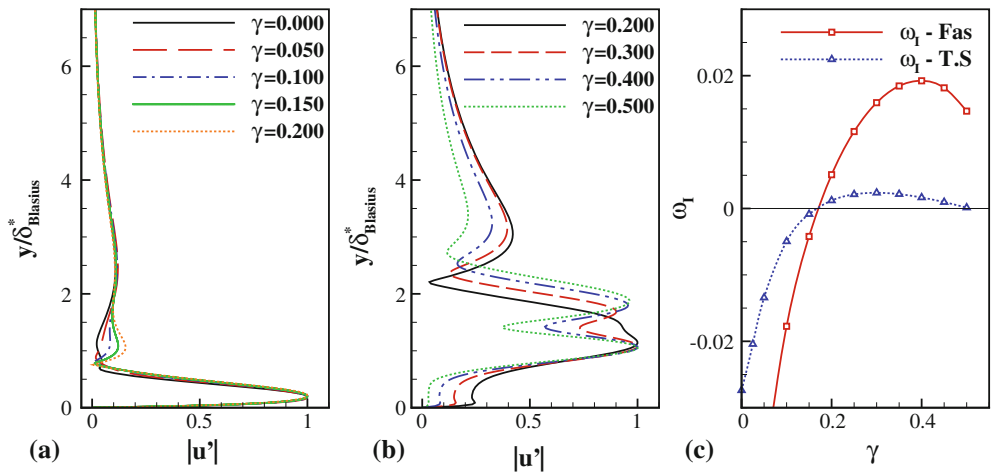

Fig. 15 Eigenmodes of the **a** slow and **b** fast instabilities for the conditions of $Re_{\delta*,\text{Blasius}} = 4{,}000$ and $\alpha = 0.5$. **c** The stability of the modes is also shown for reference

the momentum injection effects become more and more pronounced, the shape of this outer eigenmode also changes, indicating that this faster mode is strongly coupled to the momentum injection and more sensitive to the magnitude of the wall jet.

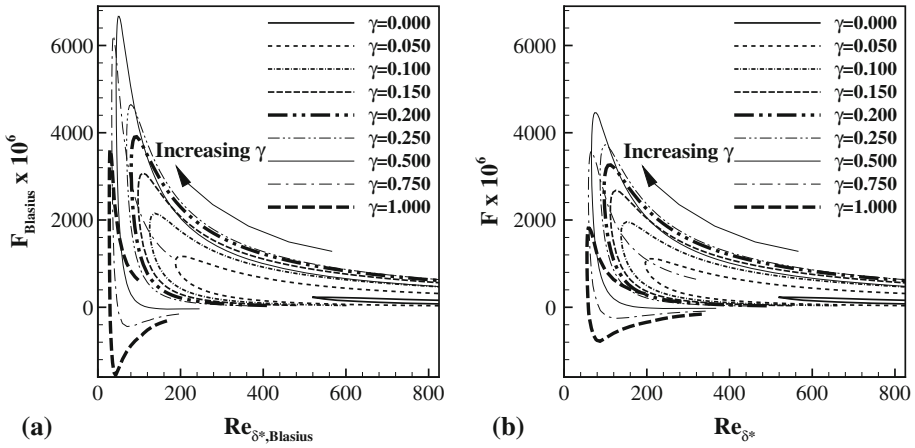

Fig. 16 Neutral stability curves of the counter flow actuated flows where $\eta = 1.0$. **a** scaled by δ^* and **b** $\delta^*_{\text{Blasius}}$

This second mode does not become relevant until the wall jet effects in the boundary layer reach a certain level. From the computations of Fjørtoft's theorem, this effect should occur at $\gamma = 0.153 \pm 0.003$. When the flow stability is examined in the inviscid limit ($Re \to \infty$) using the current eigenvalue method, the critical value is found to be $\gamma = 0.14375 \pm 0.006$. The viscid results (a sampling of which are shown in Fig. 14) indicate that the inviscid instabilities become relevant near $\gamma = 0.156 \pm 0.006$. In all, there is reasonably good agreement at what point this mode should become important between these different methods and that this mode is inviscidly unstable.

3.4 Counter flow actuation

If the plasma actuator is oriented in the opposite direction such that momentum is removed from the flow, it is expected that the boundary layer will be destabilized relative to the Blasius boundary layer profile. Neutral stability curves have been calculated for the case of counter flow operation (Fig. 16). These calculations show that this method of operation is highly destabilizing, reducing the critical Reynolds number more than an order of magnitude from $Re_{\delta^*} \approx 520$ for the Blasius boundary layer ($\gamma = 0$) to $Re_{\delta^*} < 30$ ($\gamma = -1$).

It was noted in Sect. 2 that the velocity profiles for counter flow operated plasma actuation may cause flow reversal. With this flow reversal, there is the implication that some eigenmodes of the flow may travel upstream or remain stationary. Within this subset of modes which remain stationary, the possibility of an absolute instability exists. Furthermore, the neutral stability curves (Fig. 16) indicate that for sufficiently large, negative values of γ, there are unstable modes with zero real phase velocity (as $c_R = FRe/\alpha$). However, this observation does not satisfy the more rigorous requirements of an absolute instability as defined by Briggs [27] and Bers [28]. These requirements for an absolute instability are that:

1. There exists a dispersion relationship connecting ω and α, defined as $\mathscr{D}(\omega, \alpha) = 0$. In the complex domains of ω and α, there must be saddle points where $\partial\omega/\partial\alpha = 0$, i.e., the group velocity equals zero.
2. The saddle points must be pinch points of an upstream and downstream traveling mode.
3. The saddle point must also be unstable. That is, $\omega_I > 0$ at the saddle point.

Constructing a "net map" allows for the visualization of the dispersion relationship (which is a function of the velocity profile and Reynolds number) in terms of the complex values of α and ω (Fig. 17). A saddle point is immediately visible in each of these plots. It can be seen that as the Reynolds number is increased, the value of ω_I at this point increases from negative to positive, which satisfies the third requirement for an absolutely instability. It can be seen that above a critical Reynolds number, $Re_{\delta^*,\text{abs.crit}}$, the previously convective instability becomes an absolute instability.

This absolute instability presents a conflicting view of the viscous convection instability. Measurements of the eigenvalues as shown in Fig. 13 indicate that instabilities seen with counter flow actuation are direct modifications of the Tollmien–Schlichting wave as momentum is injected in the direction opposing the free stream velocity. However, Fjørtoft's criterion (and the calculations of the flow instability in the inviscid limit) suggest that an inviscid instability should be present, even for small, negative values of γ. When one considers

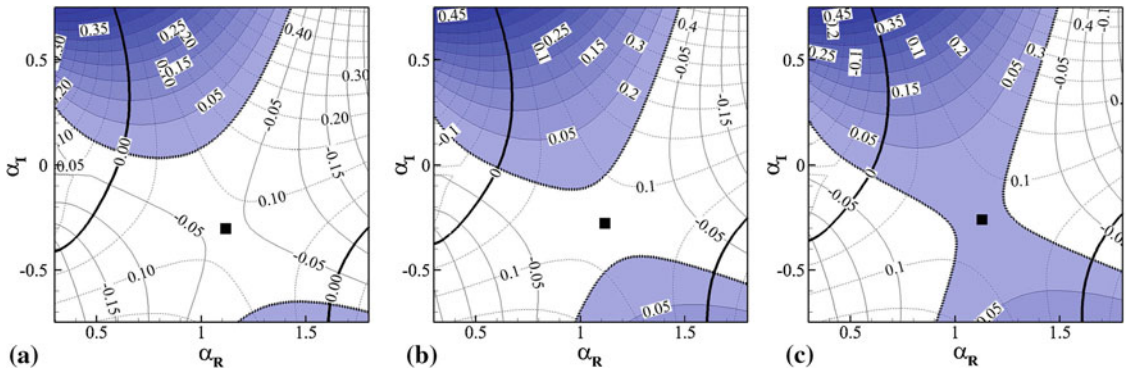

Fig. 17 Net maps for **a** $Re_{\delta^*,\text{Blasius}} = 26$, which is absolutely stable, **b** $Re_{\delta^*,\text{Blasius}} = 30$, which is convectively unstable, and **c** $Re_{\delta^*,\text{Blasius}} = 32$, which is absolutely unstable for $\gamma = -1.0$ and $\eta = 1.0$. *Solid lines* indicate the contours of ω_R. *Dashed lines* indicate the contours of ω_I. The *shaded region* is temporally unstable. The values of ω at the pinch points are **a** $\omega = 0.0926214 - i0.046581$, **b** $\omega = 0.0885969 - i0.010166$, and **c** $\omega = 0.0867067 + i0.00496014$, which are marked by the *black squares*

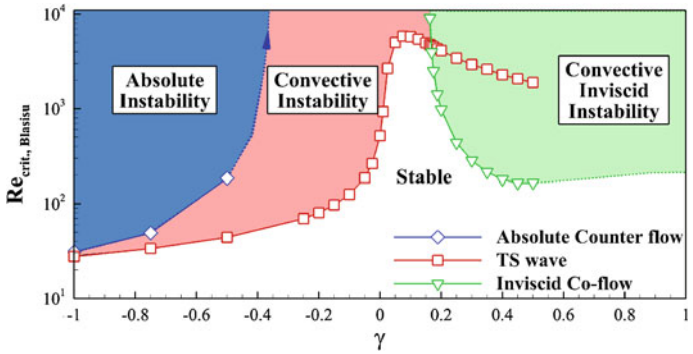

Fig. 18 A comparison of the critical Reynolds numbers of the different instabilities compared to γ for $\eta = 1$

the growth rates of instabilities occurring from counter flow operation (shown in Fig. 13), the evidence pushes more toward this instability being inviscid in its behavior. Large growth rates are normally associated with inviscid instability, and the calculated growth rates are significantly higher for counter flow actuation than they are for a normal Blasius boundary layer and other known viscid instabilities.

3.5 Comparison of the onset of different stability modes

Combining all of the stability results that have been garnered from this model of the flow, it can be seen that there exist a wide variety of phenomena that occur within the combined wall jet/boundary layer velocity profile. The different critical Reynolds numbers have been plotted as a function of γ in Fig. 18. It can be seen that the TS wave remains present for all values of γ, though for larger levels of co-flow actuation, the TS instability is stabilized relative to its importance in the Blasius boundary layer, only being present at significantly higher Reynolds numbers. The upper limit on improving the stability of the boundary layer appears to occur around $\gamma = 0.075$, with the critical Reynolds number being increased from $Re_{\delta^*,\text{Blasius}} = 520$ for the non-actuated flow to $Re_{\delta^*,\text{Blasius}} = 5{,}818$. For the counter flow actuation, the TS wave is destabilized and becomes unstable at Reynolds numbers a full order of magnitude lower than that of the Blasius boundary layer. Furthermore, for sufficiently strong counter flow actuation, an absolute instability becomes significant.

3.6 Comparison to the universal correlation

It can be seen that both co-flow and counter flow operation of the plasma actuators have a profound effect on the boundary layer stability. However, other boundary layer profile modifications can have an equally strong

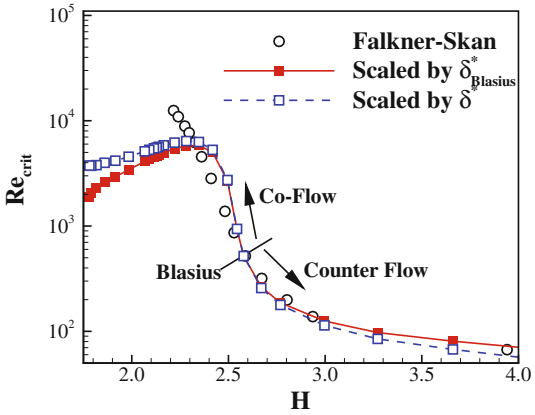

Fig. 19 Comparison of current results to other boundary layer profiles. Falkner–Skan data taken from Wazzan et al. [15]

effect on the flow stability. It is thought that there is a certain "universal correlation" between the flow stability and the shape factor [15]. It can be seen in Fig. 19 that for the convective viscid instability, the critical Reynolds numbers reached as part of this study are in agreement with other boundary layers when compared via the shape factor, $H = \delta^*/\theta$.

For small levels of actuation, these stability limits are comparable to other boundary layer profiles. However, as larger levels of plasma actuation are examined, it can be seen that they deviate from the behavior seen in other boundary layer profiles. This effect is likely due to the wall jet component of the velocity profile becoming significant relative to the boundary layer component, and transforming the flow in such a way that it cannot be compared to other boundary layers. Data is presented for the critical Reynolds number scaled by both $\delta^*_{\text{Blasius}}$ and the calculated value of δ^* for the velocity profile. The Reynolds number scaling does seem to make some difference in matching the current results to the universal correlation. However, once the velocity profile allows for significant wall-jet-like effects to develop, the critical Reynolds number diverges from that of more traditional boundary layers.

4 Qualitative comparison with experimental efforts

The present results do not initially seem to align with the existing experimental results. Experimental results show that the application of DBD plasma actuators in a steady co-flow orientation are able to stabilize the flow, but not necessarily to the degree suggested by the present analysis. Furthermore, the over-shoot seen produced by the present model is rarely seen, though experimental results have reported it [2]. Furthermore, the separated, reversed flow generated by strong counter flow actuation has never been reported in the existing literature. While these experimental results seem to disagree with the present analysis, upon closer examination, these disagreements may not actually exist.

Experimental results show that the addition of a single DBD actuator operated in a co-flow manner is able to stabilize the flow [5,6,8,14]. Furthermore, as the voltage of the actuator is increased (which implies greater momentum addition, and increased values of u_p and γ), the transition point in the flow moves farther and farther downstream [14]. This indicates that as γ is increased, the flow is stabilized. The boundary layer profiles displayed in studies showing moderate increases in boundary layer stability typically show small to moderate changes in the boundary layer profile, suggesting that the value of γ in these boundary layer profiles is moderate, largely in the range of $0.05 < \gamma < 0.25$, which is in the region of enhanced stability shown in Fig. 18 (the low velocity tests of Séraudie et al. [14] being the exception), a sample of the experimental results can be found in Table 4.

The order of magnitude increase in the critical Reynolds number also presents itself as contradictory with the experiments, as the experiments performed thus far all still transition at some point downstream. The transition eventually seen in the experimental results is due to a gradual dissipation of the momentum induced by the body force, and the boundary layer velocity profile relaxing back to the preexisting profile. As the velocity profile relaxes, the local value of γ asymptotically approaches zero. Any gains in stability due to the modification of the boundary layer profile may be lost, though gains due to a reduction in the boundary layer height because of the momentum should still remain. To achieve the incredibly high values of Re_{crit}

Table 4 Sample of experimental results showing stabilization of the boundary layer using a single co-flow-oriented plasma actuator in terms of γ_0

Study	γ_0	Geometry
Grundmann and Tropear [5,6]	0.06	Adverse pressure gradient
Séraudie et al. [14]	0.20–0.57	Airfoil (favorable pressure gradient near the actuator, adverse downstream)
Duchmann et al. [8]	0.18–0.25	Adverse pressure gradient

shown in Fig. 18, an array of distributed actuators would be necessary to generate and maintain the modified boundary layer profile, starting from below the critical Reynolds number and beyond the critical point where the boundary layer becomes unstable. To the authors knowledge, no experiments of this configuration examining the boundary layer's stability have been reported, though the stability analysis of Duchmann et al. [12] suggests that there are significant gains to be made with respect to flow stabilization.

The conditions where the plasma generated wall jet greatly overshoots the boundary layer profile are rarely seen under experimental conditions. The first reason for this plasma actuators are only able to generate velocities up to approximately 10 m/s, and many actuator geometries cannot generate flow velocities this high. As such, a wind tunnel test performed at 20 m/s could only see a maximum value of $\gamma_0 = 0.5$ and more likely a value closer to $\gamma_0 = 0.25$. When examining boundary layer profiles downstream, the localized values of γ would be even lower. However, there does appear to be some evidence that these boundary layer profiles do exist [2]. A second reason, which better reconciles the gap in experimental results with the present results, is that the boundary layer profiles that display a large overshoot are highly unstable. The present work suggests that these flow exhibit an inviscid instability long before the overshoot is present (Figs. 6, 15c). As such, even if they can be created, they will likely transition very quickly, destroying the laminar base flow. As such, the laminar flow displaying a large overshoot is somewhat of an artificial flow and should not exist naturally, except at very low Reynolds numbers or in low disturbance environments, where it is still stable.

A similar reconciliation of experimental data and stability calculations exists for the counter flow results. A counter flow-oriented plasma actuator of sufficient magnitude will likely cause the flow to reverse and separate at the location of the actuator. This separation should generate a laminar separation bubble if the incoming flow is laminar. This type of flow is known to possess an absolute instability and transition very quickly [29]. Again, for this flow to remain laminar in a natural setting is highly unlikely, due to the large growth rates, and the flow will most likely transition quickly, making it difficult to spot under experimental circumstances.

4.1 Unsteady effects

The momentum addition provided by DBD actuation is inherently unsteady, as the devices are powered by a high-frequency AC signal. Normally, the time scales associated with plasma actuation are on the order of 10's of kHz, while those associated with a low-speed flow are on the order of 100's of Hz. These two time scales are separated by two orders of magnitude, and it is often assumed that only the mean component of the momentum addition is relevant to the flow control. It should be noted that this order of magnitude approximation still based around the use of a steady flow for the stability analysis. For a more accurate analysis, the unsteady effect of the plasma actuation on the boundary layer would need to be taken into account through a Floquet stability analysis.

The present analysis of instabilities relevant to the plasma actuated flow indicates that potential inviscid and absolute instabilities may occur at significantly higher frequencies than the TS wave. As such, assumptions based on the separation of time scales must be revisited in order to establish when they may or may not be valid. The non-dimensional frequency used to characterize the present instabilities can be defined using (dimensional) parameters as

$$F = \frac{2\pi f \nu}{u^2} \tag{21}$$

may be arranged to provide an upper limit on the speed where plasma actuation is able to be used without self-exciting the flow $\left(u_{\infty,NE}\right)$. Performing this rearrangement, the upper limit is

$$u_{\infty,NE} < \sqrt{\frac{2\pi f_{\text{plasma}} \nu}{F_0}} \tag{22}$$

Table 5 Approximate non-dimensional frequencies for different instability modes and the free stream velocity where the plasma actuation will begin to excite these modes

Instability mode	$F_0 \times 10^6$	$u_{\infty,\mathrm{NE}}$ (m/s)
TS wave—co-flow	200	68.4
TS wave—counter flow	2,000	21.7
Inviscid instability	1,000	30.7

For each of the three instabilities, rough estimates of the baseline non-dimensional frequency, F_0, can be established in order to provide order of magnitude estimates as to when the plasma actuation will begin to excite these modes on its own, which are provided in Table 5. These frequencies are case specific, depending on the total level of momentum added into the flow, as well as the Reynolds number, so only approximate values are provided. For the other variables, dimensional parameters are $\nu = 1.5 \times 10^{-5}\,\mathrm{m}^2/\mathrm{s}$, and $f_{\mathrm{plasma}} = 10\,\mathrm{kHz}$. The results of this order of magnitude analysis indicate that even for relatively low-speed flows, the inviscid and counter flow actuated TS instability mechanisms may be self-excited by the plasma actuation. At moderately higher velocities (upward of 68 m/s), the DBD actuation may even excite the TS mode when co-flow actuation is employed, at which point this type of actuation is actively causing the flow to transition, not stabilizing it.

When it comes to stabilizing a flow using DBD plasma actuation, this result places an approximate upper limit on the free stream velocity where success may be found, that is, $u_\infty < u_{\infty,NE}$. However, when attempting to accelerate the laminar to turbulent transition process at higher velocities (i.e., $u_\infty > u_{\infty,NE}$), it appears that the DBD actuation has the potential to simultaneously destabilize the flow and to generate the unstable perturbations. This self-excitation may be one reason why these other instability modes have not yet been reported in the literature, and it may also provide some additional control authority at higher velocities when attempting to destabilize the boundary layer at higher velocities.

5 Conclusions

Numerically simulated velocity profiles have been used as the basis for developing a model of a boundary layer influenced by DBD actuation, based on the superposition of wall jet and boundary layer velocity profiles. In developing this model, non-dimensional parameters have been developed to characterize the velocity profiles seen in the simulations (and which could be applied to velocity profiles collected experimentally) in order to parameterize the present model the boundary layer flow. While only a zero pressure gradient boundary layer was examined in this study, the method could be easily extended to boundary layers with pressure gradients.

The velocity profiles created through this model were then examined in a number of different ways. Very basic analysis suggested the existence of absolute and inviscid instabilities, in addition to the preexisting TS instability. Using a local linear stability analysis and parametric studies, the existence of these modes was verified, and neutral stability curves were computed in order to map out where these different instabilities lie with respect to the Reynolds number and the velocity ratio of the plasma actuation to the free stream velocity. The eigenvalue method used does have some weaknesses in terms of the assumptions made. The applicability of these assumptions has been quantified based on flow fields from the simulations, and for appropriate values of the velocity ratio, these assumptions are satisfied. Closer to the actuator, and for larger values of the velocity ratio, the assumptions are not strictly satisfied, but the results of using this method still seem to confirm the existence of the predicted absolute and inviscid instabilities.

In performing these parametric studies, the domain of the different instabilities was found to strongly support destabilizing the boundary layer using co-flow or counter flow operation of plasma devices. This is good news for those who hope to use this type of plasma-based flow control to accelerate the laminar to turbulent transition process, as this flow destabilization can decrease the critical Reynolds number by more than an order of magnitude. However, it was also found that there is a distinct region of the parametric landscape which allows for significant flow stabilization, into a comparable regime as boundary layer suction. This regime, which is characterized by very slight co-flow actuation in the boundary layer ($\gamma \in (0.01, 0.2)$ for $\eta = 1$), allows for the critical Reynolds number of the boundary layer to be increased by a full order of magnitude.

Comparing these results to the existing experimental evidence, some qualitative support for the stability calculations does exist. Evidence for stabilizing the flows with reasonable levels of plasma actuation, that is, $\gamma = \mathcal{O}(0.01 - 0.1)$, can be found in several studies [5,6,8,14]. The present results suggest that the highly unstable nature of strong co-flow or counter flow actuation will not allow for these flows to exist in a laminar

form. Rather, these flows will quickly transition and will only be possible in specialized low disturbance or computational environments.

Depending on the operation of the actuator, the critical Reynolds number of the boundary layer is found to vary from an order of magnitude lower to an order of magnitude higher than that of the Blasius boundary layer. In real flow conditions, where the value of γ is likely to be $\pm\mathcal{O}(0.01 - 0.1)$, the stability effects largely line up with the universal correlation developed by Wazzan [15], which relates the shape factor and critical stability of the flow. When the addition of momentum to the boundary layer modifies the boundary layer too much, the relationship with the universal correlation breaks down and no longer applies, and though the most extreme effects of implementing plasma actuation occur outside of this region of small γ, this limited region is still important for flow stabilization and destabilization. Stabilization or destabilization effects of roughly half and order of magnitude can be seen, depending on the orientation of the actuator even with velocity ratios of approximately 0.1. If the length scale of the momentum injection to the boundary layer height were to be adjusted beyond $\eta = 1$, further improvements could likely be found, even for the limited values of the velocity ratio. Even without further optimization, and an actuator induced velocity of 5 m/s, significant gains in stability control would be made for free stream velocities of up to 50 m/s.

The present work shows that the use of plasma actuation has potential for the control of a boundary layer's stability. However, there are still a number of questions to be answered. In particular, an understanding of the stability properties in the region immediately around the plasma actuator would be beneficial. There are also questions on the non-modal growth of perturbations in the plasma actuated boundary layer, especially as the wave packets are convected over the actuator. As this flow is two-dimensional when the plasma actuator region is included in the flow domain, bi-global stability analysis should be employed in the future in order to better understand this problem. While eigenvalue formulations such as the present are useful, DNS using very specific initial conditions and/or periodic inlet conditions would allow for the examination of predetermined wave packets in the desired path to transition. Such simulations would enable a fuller understanding of how plasma actuators are able to control a boundary layer's transition process. Even though there is much more work to be done in understanding this problem, the current work presents forward progress in transition control using plasma actuators.

Acknowledgments The authors would like to thank the Computational Sciences Branch of the Air Force Research Laboratory's Air Vehicles Directorate for the use of their code, FDL3DI. The first author was supported by the University of Florida Graduate School Fellowship Award.

References

1. Roth, J.R., Sherman, D.M., Wilkinson, S.P.: AIAA Paper 1998-328 (1998)
2. Moreau, E.: Airflow control by non-thermal plasma actuators. J. Phys. D Appl. Phys. **40**, 605 (2007)
3. Jayaraman, B., Thakur, S., Shyy, W.: Modeling of fluid dynamics and heat transfer induced by dielectric barrier plasma actuator. J. Heat Transf. **129**, 517 (2007)
4. Grundmann, S., Tropea, C.: Active cancellation of artificially introduced Tollmien–Schlichting waves using plasma actuators. Exp. Fluids **44**, 795 (2008)
5. Grundmann, S., Tropea, C.: In: 46th AIAA Aerospace Sciences Meeting (2008)
6. Grundmann, S., Tropea, C.: Experimental damping of boundary-layer oscillations using DBD plasma actuators. Int. J. Heat Fluid Flow **30**, 394 (2009)
7. Gibson, B.A., Arjomandi, M., Kelso, R.M.: The response of a flat plate boundary layer to an orthogonally arranged dielectric barrier discharge actuator. J. Phys. D Appl. Phys. **45**(2), 025202 (2012)
8. Duchmann, A., Kurz, A., Widmann, A., Grundmann, S., Tropea, C.: In: 50th AIAA Aerospace Sciences Meeting (2012)
9. Duchmann, A., Simon, B., Magin, P., Tropea, C., Grundmann, S.: In: 51st AIAA Aerospace Sciences Meeting (2013)
10. Albrecht, T., Grundmann, R., Mutschke, G., Gerbeth, G.: On the stability of the boundary layer subject to a wall–parallel Lorentz force. Phys. Fluids **18**(9), 098103 (2006)
11. Duchmann, A., Reeh, A., Quadros, R., Kriegseis, J., Tropea, C.: In: Seventh IUTAM Symposium on Laminar-Turbulent Transition (2010)
12. Duchmann, A., Tropea, C., Grundmann, S.: In: 51st AIAA Aerospace Sciences Meeting (2013)
13. Riherd, M., Roy, S.: In: 51st AIAA Aerospace Sciences Meeting (2013)
14. Séraudie, A., Vermeersch, O., Arnal, D.: In: 29th AIAA Applied Aerodynamics Conference (2011)
15. Wazzan, A.R., Gazley, C., Smith, A.M.O.: Tollmien-Schlichting waves and transition: heated and adiabatic wedge flows with application to bodies of revolution. Prog. Aerosp. Sci. **18**, 351 (1979)
16. Rizzeta, D.P., Visbal, M.R., Morgan, P.E.: A high-order compact finite-difference scheme for large-eddy simulation of active flow control. Prog. Aerosp. Sci. **44**, 397 (2008)
17. Shyy, W., Jayaraman, B., Andersson, A.: Modeling of glow discharge-induced fluid dynamics. J. Appl. Phys. **92**, 6434 (2002)
18. Roy, S.: Flow actuation using radio frequency in partially ionized collisional plasmas. Appl. Phys. Lett. **86**(10), 1 (2005)

19. Boeuf, J.P., Lagmich, Y., Unfer, T., Callegar, T., Pitchford, L.C.: Electrohydrodynamic force in dielectric barrier discharge plasma actuators. J. Phys. D Appl. Phys. **40**(3), 652–662 (2007)
20. Kotsonis, M., Ghaemi, S., Veldhuis, L., Scarano, F.: Measurement of the body force field of plasma actuators. J. Phys. D Appl. Phys. **44** (2011)
21. Kriegseis, J., Schwartz, C., Duchmann, A., Grundmann, S., Tropea, C.: In: 50th AIAA Aerospace Sciences Meeting, Nashville, TN (2012)
22. Singh, K.P., Roy, S.: Force approximation for a plasma actuator operating in atmospheric air. J. Appl. Phys. **103**(1), 013305 (2008)
23. Maden, I., Kriegseis, J., Maduta, R., Jakirlíc, S., Schwartz, C., Grundmann, S., Tropea, C.: In: 20th Annual Conference of the CFD Community of Canada, Canmore (2012)
24. Opaits, D., Zaidi, S., Shneider, M., Likhanskii, A., Edwards, M., Macheret, S.: AIAA Paper 2010-0469 (2010)
25. Blasius, H.: Grenzschichten in Flüssigkeiten mit kleiner Reibung. Z. Math. Phys. **56**(1), 1–37 (1908)
26. Glauert, M.B.: The wall jet. J. Fluid Mech. **1**, 625 (1956)
27. Briggs, R.J.: Electron-Stream Interaction with Plasma. MIT Press, Cambridge, MA (1964)
28. Bers, A.: Linear Waves and Instabilities. In: Plasma Research Report. Research Laboratory of Electronics, Massachusetts Institute of Technology (1972)
29. Hammond, D.A., Redekopp, L.G.: Local and global instability properties of separation bubbles. Eur. J. Mech. B Fluids **17**(2), 145–164 (1998)